Available online at www.sciencedirect.com
SCIENCE DIRECT®
Journal of Molecular Graphics and Modelling 23 (2005) 447–456
Journal of Molecular Graphics and Modelling
www.elsevier.com/locate/JMGM

Structure and property correlation for Ag deposition on α-Al_2O_3—a first principle study

Abhijit Chatterjee [a,b,*], Syuichi Niwa [b], Fujio Mizukami [b]

[a] *Accelrys K.K., Nishishinbashi TS Bldg. 11F, 3-3-1 Nishishinbashi, Minato-ku, Tokyo 105-0003, Japan*
[b] *Laboratory of Membrane Chemistry, National Institute of Advanced Industrial Science and Technology, AIST Tohoku, 4-2-1 Nigatake, Miyagino-ku, Sendai 983-8551, Japan*

Received 21 October 2004; received in revised form 18 January 2005; accepted 18 January 2005

Abstract

The nature of bonding at the interface between deposited silver and (0 0 1) surface of α-Al_2O_3 for both Al-terminated and OH-terminated has been investigated using a periodic ab initio method. Substantial inter-planar relaxations within the alumina were found at both the interfaces and the bulk. The periodic calculation with Ag deposition shows that 10% of Ag loading on alumina results maximum stability. Now, this is known that, the clean alumina surface only exists at UHV condition and normally the alumina surface prefers to stay hydroxylated. We have therefore compared the silver bonding over hydroxylated alumina surface and confirmed the fact that the hydroxylated surface binds silver weakly in comparison to the clean surface and it recommends that the silver cluster over the hydroxylated surface begins to join in to form three-dimensional nuclei. The deposited Ag forms a cluster on top of the alumina surface. The Ag atomic packing was monitored to rationalize the role of packing on activity of silver. Three low-index Ag surfaces (1 0 0), (1 1 0) and (1 1 1) are investigated via the ab initio density functional calculations with ultrasoft potentials. We have monitored the relation between Ag atomic packing and its electronic properties. The results show that the structural and electronic property of Ag deposited on alumina surface depends significantly on atomic packing. Ag(1 1 0) over clean alumina surface shows highest surface energy and smallest work function, whereas for the OH-terminated surface it is the Ag(1 1 1). The results are discussed in view of the existing experimental data and models of metal–oxide interface.

Keywords: Structure and property correlation; Ag deposition; First principle study; Alpha-alumina; Ag atomic packing; CASTEP

1. Introduction

The understanding of the nature of noble metal/metal–oxide interface constitutes one of the most intriguing challenges nowadays for the material scientists. The metal–ceramic-based materials play a significant role in catalysis, photolysis and photooxidation reactions, electrocatalysis, and gas sensors, etc. [1–4]. Aluminum oxide is one of the most widely used supports for catalytic purposes because of both its mechanical and thermal resistance. Experimental studies in this field are complicated by difficulties in preparing stoichiometric single-crystal surfaces and by the sheer complexity of the bulk and surface oxide structures. It has been proved already that, although, aluminium-terminated surfaces may exist under vacuum [5,6], it is likely that surfaces exposed to oxygen and water have different terminations. High-resolution electron-energy-loss spectroscopy (HREELS) experiments by Coustet and Jupille [7] indicate that, OH groups on the hydroxylated (0 0 1) surface occupy positions consistent with a perfect oxygen-terminated surface. The major experimental advances in terms of STM [8] and microcalorimetry [9] helped to understand the growth of high-quality thin oxide films on conducting substrates and to measure the heat of adsorption of metal vapor on oxide films, respectively.

Until recently, the understanding of bulk, surfaces and interfaces of oxides lagged far behind than that of semiconductors and metals [10,11]. This was partly due to experimental difficulties and partly because of the complexity of many oxide materials, made them difficult

* Corresponding author. Tel.: +81 3 3578 3861; fax: +81 3 3578 3873.
E-mail addresses: c-abhijit@aist.go.jp, achatterjee@accelrys.com (A. Chatterjee).

1093-3263/$ – see front matter © 2005 Elsevier Inc. All rights reserved.
doi:10.1016/j.jmgm.2005.01.002

to study with accurate theoretical methods. Previously, ab initio calculations on the energetic and relaxed structure of an oxide surface were made on MgO(0 0 1) using Hartree–Fock (HF) theory [12]. HF calculations have since been used on several other oxides [13–17]. DFT (density functional theory) methods have begun its venture in oxides somewhat later but progressed in a rapid manner; hence, a number of studies have been reported in the last decade on oxides as well as other materials [18–25]. In the last couple of years, there have been considerable progresses in the area [26–32] of electronic and structural properties of mixed metal oxides using first principle density functional theory.

A recent study of Verdozzi et al. [33], which is the first accurate theoretical study of metals on sapphire found two very different adsorption mechanisms, depending on the coverage. While isolated adatoms are oxidized and bind strongly as ions, but if coordinated to two or more other metal adatoms, the adsorbates are metallic, showing negligible charge transfer to the surface and relatively weak adsorption, mainly by polarization. They performed a local density approximation (LDA) calculation for structural and electronic properties of sapphire(0 0 1) clean and with d-metal overlayers, which show the significant surface relaxations penetrate to the third oxygen layer, 5.2 Å below the surface. But the above-described method has its own limitation in terms of the definition of clean sapphire surface itself. Eng et al. [34] have shown that the reactivity of the UHV clean α-Al_2O_3 surface should differ markedly from an alumina surface prepared in presence of water. The surface Al sites in the Al-terminated model are strong Lewis acid sites, whereas the OH groups in the OH-terminated surface are Lewis bases. After hydroxylation of the alumina surface, all surface sites become Lewis bases with lowered reactivity to water but enhanced overall reactivity toward metals. There was as well a reaction dynamics of water on alumina surfaces by first principle calculations reported by Hass et al. [35]. It has covered mainly the complex dynamics of water dissociation and related surface reactions. Kelber and co-workers [36] and Chambers co-workers [37,38] have shown that no clean sapphire surface exist except UHV. The clean sapphire surface is the normal terminated alumina surface [39]. The (0 0 1) surface consists of one Al ion for every three O ions. The terminal Al ions are only slightly above the plane of the plane of close-packed oxygen. Jennison and Mattsson [40] have extended the work of Chambers et al. [38] to a number of metals using first principle calculations and concluded that room-temperature process for creating metal–oxide interfaces discovered by Chambers et al. on fully hydroxylated alumina, is a general phenomenon and could have many applications involving different metals. Kelber et al. [41] in one of their earlier paper had observed that the Cu growth on a partially hydroxylated α-Al_2O_3(0 0 1) surface is dominated by two-dimensional island formation, whereas Cu growth on dehydroxylated surfaces is likely dominated by three-dimensional island formation. Hass et al. [42] has explored Al-terminated α-Al_2O_3 surfaces with varying degrees of water coverage using molecular dynamics. They have as well used clusters to locate the adsorption behavior of the water molecule. First principle density functional calculations were performed to study metal adsorption (Li, K, Y, Nb, Ru, Pd, Pt, Cu, Ag, Au and Al) at 1/3–4 monolayer coverage atop Al_2O_3 films on Al(1 1 1) [43]. Recently, we have used density functional theory to correlate layer charge and catalytic activity of dioctahedral smectites [44] and also monitored the location and activity of RuO_2 in alkali-metal hexatitanate using first principle study [45]. To the best of our knowledge, there is no systematic study about the structure and property correlation of deposited Ag on α-Al_2O_3 surface.

The current study aims to rationalize the phenomenon of Ag deposition on α-Al_2O_3 and also to correlate the structure and property of Ag, deposited on the Al_2O_3 surface. We first studied the Ag loading over alumina(0 0 1) surface, to locate the optimum loading from 1/3 to 1 ML, where we assume 1/3 ML = 1 metal atom per surface oxygen atom for both Al-terminated and OH-terminated alumina surface. This has been followed by the calculation of low-index Ag surfaces to monitor the role of surface packing on the activity. The interactions of low-index silver surfaces with both the clean and hydroxylated alumina surface are compared. The results as well propose the nature of the bonding of silver with α-Al_2O_3.

2. Method and model

Ab initio total energy pseudopotential calculations were performed using CASTEP (Cambridge Serial Total Energy Package of Accelrys Inc.) and associated programs for symmetry analysis, that has been described elsewhere [46,47]. In this code, the wave functions of valence electrons are expanded in a basis set of plane waves with kinetic energy smaller than a specified cutoff energy (E_{cut}). The presence of tightly bound core electrons is represented by non-local ultrasoft pseudopotentials [48]. CASTEP is a pseudopotential total energy code that employs Perdew and Zunger [49] parameterization of the exchange-correlation energy, supercells and special point integration over the Brillouin zone and a plane wave basis set for the expansion of wave functions. The methodology has been used in mineralogy to examine the hydration of corderite [50]. Becke–Perdew parameterization [51,52] of the exchange-correlation functional, which includes gradient correction (GGA), was employed. The pseudopotentials are constructed from the CASTEP database. The screening effect of core electrons is approximated by local density approximation (LDA), while the screening effect of valence electrons is taken care off by GGA. Reciprocal space integration over the Brillouin zone is approximated through a careful sampling at a finite number of k-points using the Monkhorst–Pack scheme [53]. In all calculations, the

kinetic energy cutoff (E_{cut}) and the density of the Monkhorst–Pack k-point mesh were chosen high enough (here we used symmetric five k-points) in order to ensure the convergence of the computed structures and energetic. The basis cutoff used is 380.0 eV. The energy tolerance is $5.0e^{-6}$ eV/atom, the force tolerance is 0.01 eV/Å, and the displacement tolerance is $5.0e^{-4}$ Å. To obtain equilibrium structures for a given set of lattice constants, ionic and electronic relaxations were performed using the adiabatic or 'Born–Oppenheimer' approximation, where the electronic system is always in equilibrium with the ionic system. Relaxations were continued until the total energy had converged.

We have calculated the surface energy and work function for low-index surfaces of silver before and after deposition over α-Al_2O_3 to monitor the role of atomic packing on the activity of silver.

The surface energy per surface atom is calculated as follows [54]:

$$\sigma = \tfrac{1}{2}(E_{slab} - NE_{bulk})$$

where E_{slab} and E_{bulk} are the total energies for the slab (the cell containing N atoms) and for bulk crystal (with a primitive cell), respectively. 1/2 is used, as there are two surfaces in the slab model.

Work function is calculated as:

$$\varphi = E_{vac} - E_F$$

where E_{vac} and E_F are vacuum energy and Fermi energy, respectively. The vacuum energy is estimated by averaging the electrostatic potential over the middle plane of the vacuum layers.

Total energy calculations were performed on a supercell with periodic boundary conditions, which enables us to use a basis of plan waves. The supercell has the form of a rhombohedral prism, and in the stoichiometric slab it contains 30 atoms. This slab is exactly the thickness of one bulk unit cell of the corundum structure. Our surface calculations were performed on slabs repeated periodically in the z-direction, with a vacuum space of thickness about equal to the slab. Fig. 1 shows the structure with labeled atoms. Only the top two surface aluminum and with their three neighboring oxygen were relaxed in the parent structure for Al-terminated surface, while for OH-terminated surface the top OH layer with the aluminum layer and its nearest-neighbor oxygens were relaxed. The slab was hydroxylated on one surface. The opposite side of the slab was kept frozen at positions for the surface. This is necessary since a bulk-terminated surface is not stable due to its large surface dipole, which causes very large relaxations to occur [33,40] on this surface, which consists of three O ions per unit cell and one Al ion slightly above the O plane. Periodically repeated slab supercells with 11 layers separated by 9 layers of vacuum were used to model the Ag(1 × 1) surface.

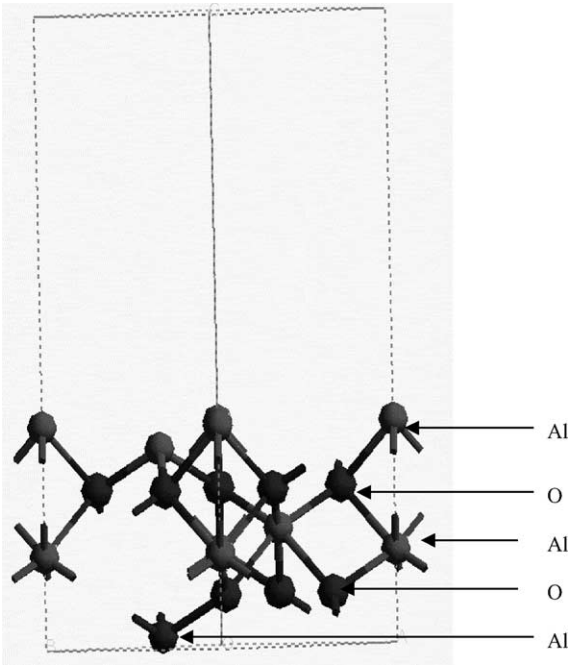

Fig. 1. The periodic slab model representing α-Al_2O_3 with all the atoms labeled. The bottom two layers were fixed throughout the calculation.

3. Results and discussion

Our aim is to rationalize the structure of silver over α-Al_2O_3(0 0 1). We have performed the calculation for both Al-terminated and OH-terminated surface. So, first we loaded silver with increasing concentration from 1/3 to 1 ML and optimized the structure. The cell parameters were measured. The results shown in Tables 1 and 2 represent the calculated metal surface binding after each Ag loading. We studied the various possible low-index structures of silver at it highest loading to monitor the effect of packing on activity. The surface energy and work function for the set of structures are shown in Table 3. The effect of packing on

Table 1
Cell parameters for α-Al_2O_3 and for the aluminum lattices after incorporation of silver along with a reference to the results obtained by experiment for α-Al_2O_3

Molecule	a	b	c	α	β	γ
Al-α-Al_2O_3	4.78	4.78	12.88	89.96	89.94	120.16
Experiment	4.75	4.75	12.99	90.00	90.00	120.00
OH-α-Al_2O_3	4.76	4.76	12.99	89.91	89.87	120.76
Experiment	4.75	4.75	13.09	90.00	90.00	120.00
Ag_1-alumina[a]	4.73	4.76	12.47	90.30	89.74	120.10
Ag_1-alumina[b]	4.78	4.79	12.32	90.21	89.65	120.65
Ag_2-alumina[a]	4.81	4.81	12.52	90.11	89.88	120.32
Ag_2-alumina[b]	4.83	4.84	12.46	89.89	89.57	120.54
Ag_3-alumina[a]	4.91	4.88	12.69	87.31	91.34	120.44
Ag_3-alumina[b]	4.93	4.94	12.53	88.54	89.51	120.18

[a] Al-terminated alumina surface.
[b] OH-terminated alumina surface.

Table 2
Total energy and binding energy for alumina lattices with silver

Periodic cell	Total energy (eV)	Binding energy (eV)	$E_{binding} - E_{coh}$ (eV)
α-Al_2O_3	−127.154		
OH-α-Al_2O_3	−124.455		
Blank silver	−15.057		
1/3 ML of Ag-alumina[a]	−149.122	−6.91	−5.35
1/3 ML of Ag-alumina[b]	−148.852	−9.34	−4.26
2/3 ML Ag-alumina[a]	−165.827	−8.55	−3.41
2/3 ML Ag-alumina[b]	−162.209	−7.64	−3.04
1 ML Ag-alumina[a]	−181.531	−9.20	−2.79
1 ML Ag-alumina[b]	−174.946	−5.32	−1.12

[a] Al-terminated alumina surface.
[b] OH-terminated alumina surface.

Table 3
Surface energy (σ) and work function (φ) of Ag cluster calculated using GGA and LDA functional and compared with experiment

Cell	σ (eV/atom)					φ (eV)				
	GGA	LDA	Experimental [62]	Al-Al_2O_3	OH-Al_2O_3	GGA	LDA	Experimental [61]	Al-Al_2O_3	OH-Al_2O_3
Ag(1 1 1)	0.357	0.530	0.55	0.489	0.923	4.65	4.98	4.46	5.73	6.23
Ag(1 0 0)	0.432	0.633	0.88	0.591	0.742	4.33	4.82	4.22	5.41	6.71
Ag(1 1 0)	0.649	0.952	1.18	0.862	0.612	4.30	4.66	4.14	5.17	7.11

both the clean and the hydroxylated aluminum surface were compared.

3.1. Electronic structure of α-Al_2O_3 with and without Ag deposition using CASTEP

The (0 0 1) surface of α-Al_2O_3 terminates a layered structure, in which each oxygen plane in the bulk has an associated Al plane at a distance of 0.838 Å above and below, forming a stoichiometric triple layer. The most convenient unit cell is a rhombohedral prism comprising three such (0 0 1) oxygen planes separated by the associated pairs of Al planes. The oxygen planes are separated by 2.166 Å and form a hexagonal lattice with ABABAB... stacking. Their positions are slightly laterally distorted from ideal hexagonal sites. The Al atoms occupy two-thirds of the octahedral holes in the oxygen sublattice, at the positions, which alternate between below and above the centers of these holes. The unoccupied octahedral holes are themselves stacked on a face-centered cubic lattice, ABCABC. A C3v symmetry axis passes through each Al atom and through the centers of the unoccupied octahedral sites. The stoichiometric slab has two equivalent surfaces, which are terminated by an Al plane, as in Fig. 1. The termination defines the stoichiometric surface, because the slab as a whole is stoichiometric and has two equivalent surfaces.

The possibility of uniform OH-termination of α-Al_2O_3(0 0 1) has been proposed in a number of earlier studies [35,55]. Every Al in this model remains octahedrally coordinated, while every terminating OH group bridges to two interior Al. The OH coordination is thus identical to that in the bulk aluminum hydroxides (it coordinates to Al in two out of every octahedral sites between close-packed OH layers), except that in the hydroxides, the OH groups contribute to structural integrity through interlayer hydrogen bonding. The stability of the hydroxylated surface occurs due to the fact that the primitive unit cell having three OH ions, has the same charge (−3) as the sapphire surface plane with three O^{2-} ions and one Al^{3+} ion per unit cell [34]. In our calculation, both the model used are neutral. Jennison and Mattsson [40] has proposed that the conversion from clean sapphire to the hydroxylated surface might have occurred due to water dissociation, assisted by a physisorbed layer that helps molecules find the chemisorbed sites that dissociate at room temperature. Surface Al is likely removed by the formation of $Al(OH)_3$ molecules.

We first optimized the aluminum lattice and the energy value is calculated using GGA (Table 1). The results for Al-terminated surface are in match with the numbers generated by Wang et al. [56] and Batirev et al. [57]. It is observed that the planar relaxations are quite large, while the O ions and the Al ions remain essentially coplanar within ∼0.02 Å. The relaxation of surface Al is accompanied by a 9% reduction in the length of bond (1.687 Å) to the second layer oxygen, which is less than the experimental value of ∼4% [58]. The reduction is a natural consequence of the reduced coordination of surface Al. Coordination with the outermost O atoms also causes a shortening of bonds to interior Al neighbors (1.804 and 1.889 Å). These reductions result in part for the small lateral displacements within the O layer, which manifest them primarily as slight distortions and rotations of the triangles of O atoms below each surface Al.

The predicted lateral displacement pattern qualitatively matches with the experimental values [56].

Every Al in the OH-terminated alumina model remains octahedrally coordinated, while each terminating OH bridges to interior Al. It is observed that one out of three hydroxyl groups remain parallel to the surface and form long hydrogen bonds (1.8–2.2 Å) to the neighboring O sites across the regions. The other two of the three hydroxyl groups point nearly perpendicular to the surface and have a shorter average bond length (0.95–0.97 Å). In contrast to the large relaxation that occurs upon Al termination, the outermost Al and O layers do not relax to any appreciable extent on OH-terminated α-Al_2O_3(0 0 1). The cell parameters are shown in Table 1. It is observed that OH-terminated surface has a larger vertical relaxation compared to that of Al-terminated surface.

We loaded one silver atom per surface oxygen atom or one silver atom per three surface oxygen atoms (1/3 ML) and modeled until three silver atoms saturating the surface oxygen resulting 1 ML, where three surface oxygens on the surface has three silvers. After each loading of silver, the upper three layers of the structure including the silver are optimized. The structure of alumina surface with two silvers (2/3 ML) and three silvers (1 ML) before and after optimization is shown in Figs. 2–5 for both Al-terminated and OH-terminated surface, respectively. The results of cell parameters as shown in Table 1 depicts that with increase in Ag loading the cell parameters varies in an increasing note with very few exceptions. The interesting feature is that, with the increase on Ag loading there is a vertical quench observed in both the cases, but the quenching is more pronounced in OH-terminated surface. If the metal overlayer grows beyond 1 ML, the newly deposited atoms increase the coordination of and thereby stiffen the metal film interface, rendering it as bulk like; hence, we did not perform anymore loading beyond 1 ML. This optimized silver sits just on top of the hexagonal whole comprised with aluminum and oxygen. In case of 2/3 ML silver loading, the optimized silver comes closer to each other by a distance of 1.87 Å, whereas in case of 1 ML silver loading the optimized distance is 1.78 Å, for the Al-terminated surface. The results are as well shown in Figs. 2 and 3, respectively. The silver atoms are connected to show the formation of the cluster. The average Ag–O distance is 2.43 Å, which is pretty much close with experimental values (2.45 Å) and better than that of Verdozzi et al. [33]. Silver atom is having a stronger bonding with α-Al_2O_3 surface that is largely caused by metal polarization. The aluminum and oxygen in clean relaxed α-Al_2O_3 are nearly coplanar (d_{12} = 0.04 Å), thereby neutralizing the surface polarity. The pattern changes significantly upon metal adsorption. The oxygen atom relaxes onwards by 0.3–0.5 Å and forces the aluminum ions to displace inward. This effect is much more pronounced at 1 ML resulting in a favorable Ag–O bonding. Interestingly, the Al and O ions over the clean relaxed oxide surface are nearly coplanar. After the metal adsorption, this changes dramatically. The oxygen atoms relax outwards by 0.2–0.5 Å. The large O–Al plane distance is observed for 1/3 ML situation. In the case of 1/3 ML, the high relaxation is a result of small size of Al cation and the repulsion resulted from the Ag ad ion. This further enhances the electrostatic potential of the adsorption site and the surface polarity decreases for 1 ML, as the layer over surface metal is neutral.

In case of the OH-terminated surface, the situation with 2/3 and 1 ML of Ag loading is shown in Figs. 4 and 5, respectively. The results show a very intricate phenomenon,

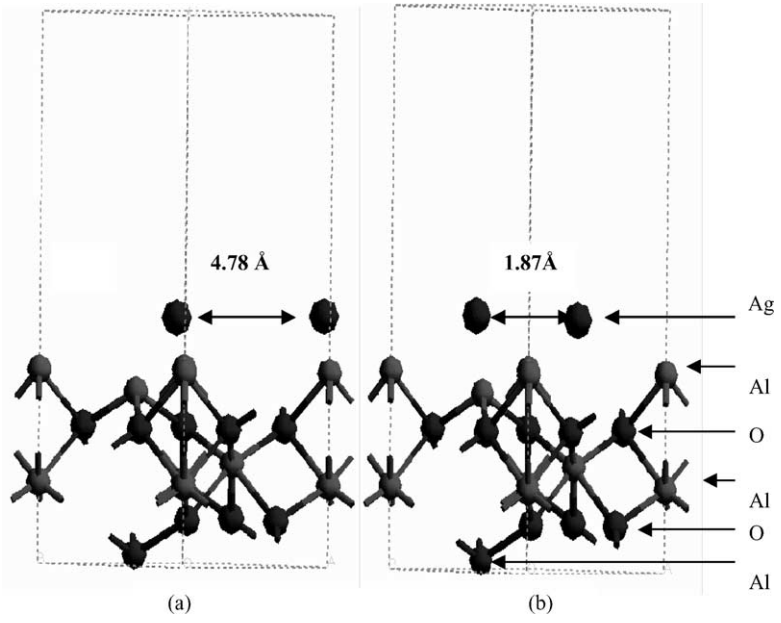

Fig. 2. The structure of clean α-Al_2O_3 with 2/3 ML silver loading before (a) and after (b) optimization. The bottom two layers were fixed throughout the calculations.

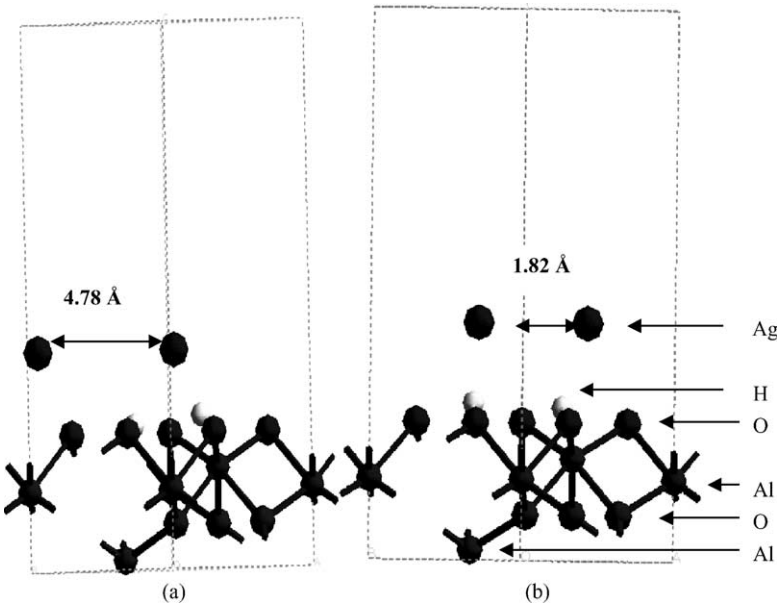

Fig. 3. The structure of hydroxylated α-Al_2O_3 with 2/3 ML silver loading before (a) and after (b) optimization. The bottom two layers were fixed throughout the calculations.

the Ag–Ag distance for 2/3 ML is 1.82 Å, which is little less than that for the Al-terminated surface with same loading. The vertical distance with the surface oxygen is increased to 2.65 Å, showing a tendency of the Ag to form a weaker bond with OH-terminated surface in comparison to clean alumina surface. The increase in Ag–Ag distance might have resulted from the repulsion of the Ag with the surface hydroxyls. This repulsion then, forces the silver to move out from polarized oxygen surface. The situation can be better understood from the surface with 1 ML of Ag coverage. It is observed that the third oxygen is moving away from the central plane and try to form a metal island. The Ag–Ag distance becomes little longer to about 1.92 Å and the Ag–O distance remains as long as 2.65 Å for the two silvers as shown in Fig. 5 and the third one moves out to about 2.74 Å. It is as well observed that with increase in Ag loading the Ag-Ag interaction predominates. The above results from the geometric parameters show that the OH-terminated surface binds the Ag less favorably than the Al-terminated surface. Now to rationalize the geometrical observations one need to study the energetic of the systems.

The total energy of the isolated system along with the system including adsorbed silver and binding energy of the silver with each loading is studied and has been shown in

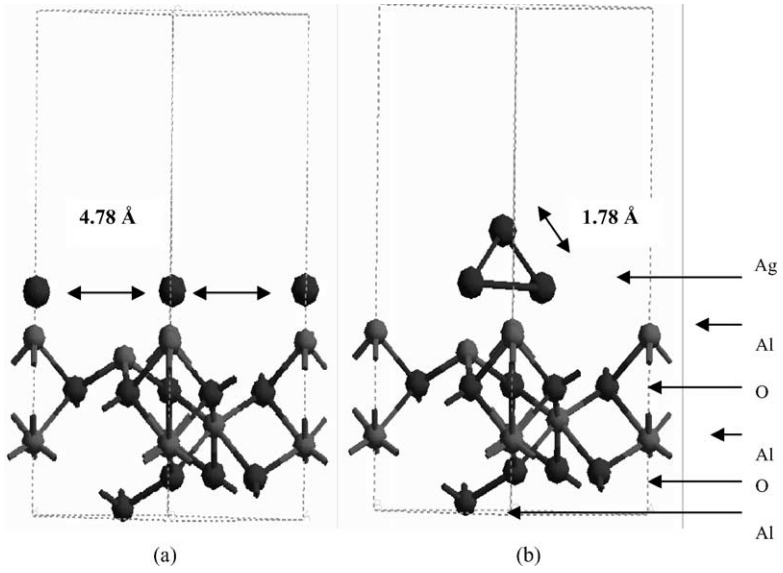

Fig. 4. The structure of clean α-Al_2O_3 with 1 ML silver loading before (a) and after (b) optimization. The bottom two layers were fixed throughout the calculations.

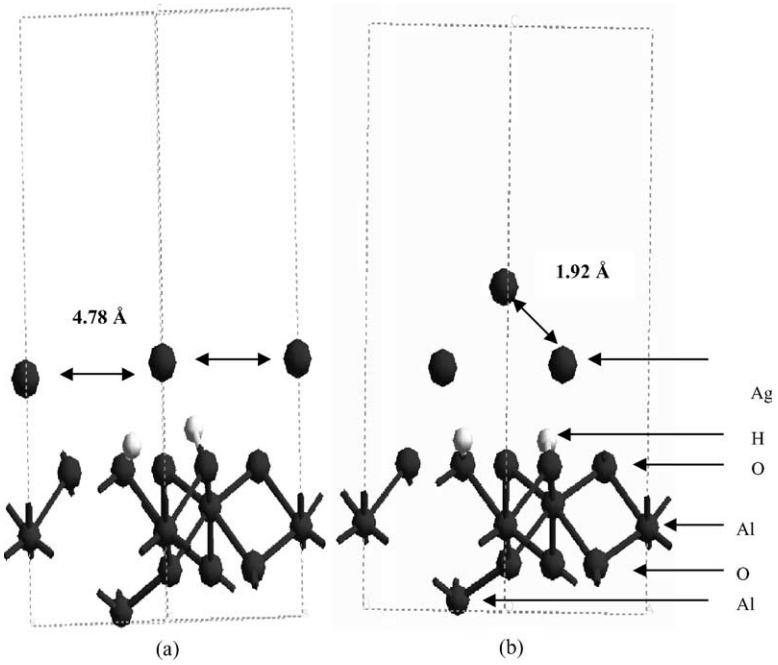

Fig. 5. The structure of hydroxylated α-Al_2O_3 with 1 ML silver loading before (a) and after (b) optimization. The bottom two layers were fixed throughout the calculations.

Table 2. The binding energy for metals over the alumina surface is calculated as the following:

$$E_{\text{binding}} = \frac{NE_{\text{metal}} + E_{\text{slab}} - E_{\text{total}}}{N}$$

where E_{binding} is the binding energy per metal atom binded to the alumina surface, E_{metal} is the energy of isolated metal atom, N is the number of metal atoms, E_{slab} is the energy of the slab and E_{total} is the total energy of the metal adsorbed alumina system. Hence, the binding energy is defined as positive, if the total energy decreases when the metal atom is brought from infinity and placed onto the surface.

For Al-terminated surface, the lattice with 1 ML of silver shows highest binding energy in comparison to that with 2/3 ML silvers on surface and 1/3 ML of silver loading on surface. This increase in binding energy with increasing coverage may be because of the adatoms are polarized by the surface, and as a result they form non-negligible dipoles on the surface. The higher the coverage, the more pronounced the dipole–dipole repulsion among co-adsorbed silver atoms. In the last column, we report $E_{\text{binding}} - E_{\text{coh}}$, i.e. the difference between binding energy and the cohesive energy of the bulk silver. A negative value suggests that the formation of a three-dimensional island of the silver metal is more favorable than the formation of a single overlayer on the oxide surface. This result of 2.85 eV is much better than the cohesive energy computations of Philipsen and Baerends [59], who found a GGA fully relativistic energy for Ag of 2.37 eV as compared to an experimental value of 2.95 eV.

For the OH-terminated surface, the binding energy for 1 ML coverage of Ag is the highest and the binding energy decreases with Ag loading, showing that the Ag bonding on OH-terminated surface will be much weaker than that of Al-terminated surface. The presence of hydroxyl groups greatly influences the binding of Ag to alumina surface. Another feature observed from Table 2 is the difference of binding energy and cohesive energy. Here, we observed again a negative value of 1.12 eV for the highest Ag coverage on OH-terminated surface. This value is comprehensively lower than that of Al-terminated alumina surface (0 0 1). There is no available experimental data to confirm this phenomenon. Kelber et al. in their work [41] with Cu deposition over alumina surface had shown that hydroxylated surface favors two-dimensional island formation, which may then act as a kinetic barrier to three-dimensional island formation. As so far we have not explored this with silver, we are unable to comment on this phenomenon as observed in case of Cu, but we are planning to monitor this in our future studies. At this point, we see weaker silver binding over hydroxylated surface in comparison to the Al-terminated surface validating the proposition of Chambers et al. [38].

3.2. Surface energy for the different Ag packing over alumina surface

We have seen from our periodic calculation that the silver at its highest loading resides as a three-dimensional cluster over both the Al-terminated alumina surface and OH-terminated surface. A set of calculations was performed with both the surfaces to rationalize the role of Ag packing with the surfaces. For Ag three high symmetry low-index

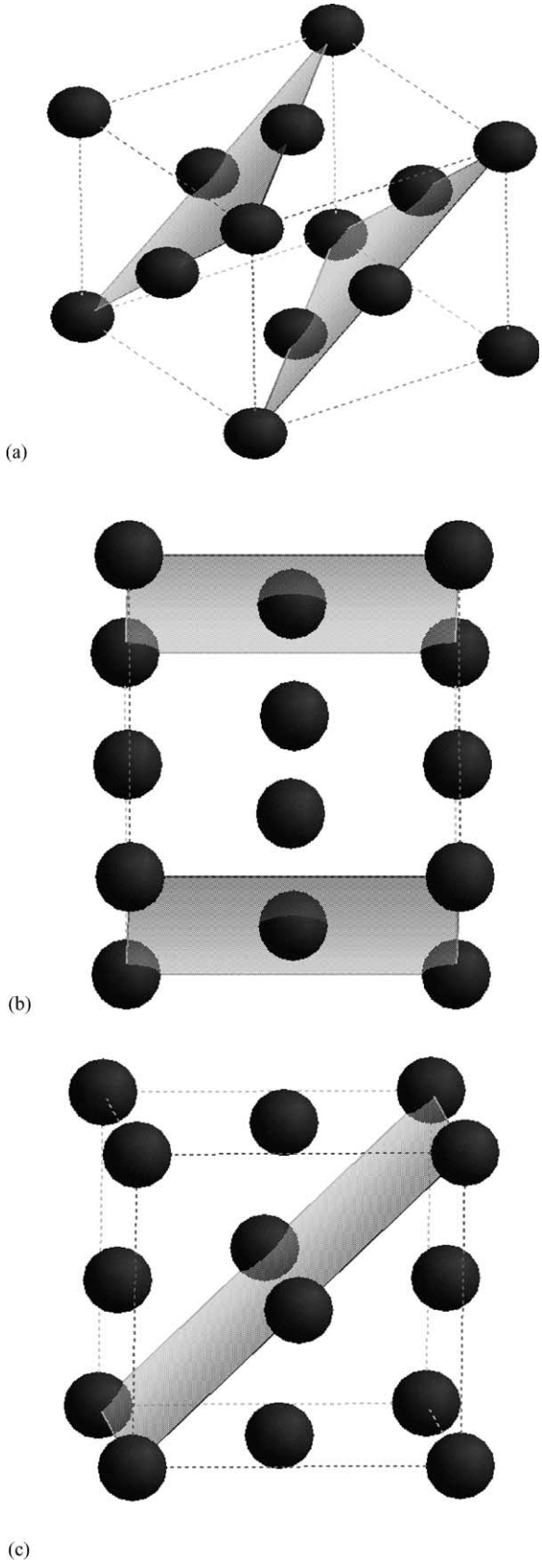

Fig. 6. The atomic packing of the silver surfaces along different low-index surfaces: (a) (1 1 1), (b) (1 0 0) and (c) (1 1 0) surfaces.

surfaces, (1 1 1), (1 0 0) and (1 1 0) have been studied. The structure is shown in Fig. 6. The Miller planes are drawn to identify the structural orientation obtained after different low-index packing. The Ag(1 × 1) surface systems are modeled using periodically repeated supercells; with 11 layers separated by 9 layers of vacuum elongated slab. First, we calculated the surface energy per surface atom for each surfaces and as well we calculated the work function for each surfaces (Table 3). We calculated the surface energy and work function for the Ag surfaces only. Those numbers are in close agreement with experiment [60,61]. In experiment, the surface energy and work function, was calculated by low-energy electron diffraction (LEED), high-energy ion scattering (HEIS), medium-energy ion scattering (MEIS) and Auger electron spectroscopy (AES) methods. Even we figured out that for the surface energy, the LDA results are in close agreement with the experimental values, whereas for the work function GGA is a better performer. So for all the cases, the surface energy and the work functions were obtained by using LDA and GGA calculations, respectively. The results are also included in Table 3. First, for the Al-terminated surface, a totally opposite trend for surface energy per atom and the work function was found. For the surface energy, the values increases in the order of Ag(1 1 1) < Ag(1 0 0) < Ag(1 1 0); on the contrary, in terms of work function, the order is Ag(1 1 0) < Ag(1 0 0) < Ag(1 1 1). Now, in terms of both it can be proposed that the activity of silver is related with nature of packing over alumina surface. The highest surface energy can also partially interpret their better activity towards molecular oxygen adsorption on the (1 1 0) surface, which projects the suitability of these surfaces for catalytic reactions on metal surfaces [62]. Because of similar structural parameters, such as interlayer distance, surface roughness, both the (1 0 0) and (1 1 1) surfaces show similar characters. However, the properties of the Ag(1 1 0) surface differ from those of the (1 1 1) and (1 0 0) surfaces. Being on the top of the alumina, Ag(1 1 1) surface has a long-range interaction with the oxygen of alumina and a short-range interaction with on top alumina.

For the OH-terminated surface, the order is different form that of Al-terminated surface. Both the order in terms of surface energy and work function is same in terms of the interacting Ag surfaces. The order is Ag(1 1 0) < Ag(1 0 0) < Ag(1 1 1). The difference in behavior is due to the difference surface architecture of the OH-terminated surface. Again, here the hydroxyl group is responsible for the difference in surface interaction scenario. The Ag(1 1 1) is favoring a long-range interaction with Al-terminated surface while it is favoring a short-range interaction with OH-terminated surface. For the first case, the surface energy is low and the work function is high, understandably both the surface energy and work function are higher for OH-terminated surface.

The results clearly demonstrated that the different atomic packing over the alumina could result different activity.

The different structural and electronics properties can therefore lead to different performance of the three surfaces for the catalytic reactions.

4. Conclusion

This is the first systematic study to monitor the silver deposition on α-Al_2O_3. We have monitored that 1 ML of silver or 10% loading of silver on α-Al_2O_3 results in the instability to the structure, to make it active for the reaction. The silver atoms form a cluster over the Al layer of α-Al_2O_3 just on top of the hexagonal hole. The results as well show that due the upward relaxation of oxygen layer, the top aluminum is relaxed inwards. The silver bonding and activity is much more dependent on the structural relaxation of α-Al_2O_3. Now, as it is known that the clean alumina surface only exists at UHV condition and normally the alumina surface prefers to stay hydroxylated. We have therefore compared the silver bonding over hydroxylated alumina surface and confirmed the fact that the hydroxylated surface binds silver weakly in comparison to the clean surface and it recommends that the silver cluster over the hydroxylated surface joins in the formation of three-dimensional nuclei. This brings us to look at the effect of silver packing on both the surfaces. Our final aim is to use the silver-coated surface for some typical catalytic reaction. The Ag atomic packing was monitored to rationalize the role of packing on activity of silver. It was observed that Ag(1 1 0) surface is the best performer in terms of activity if deposited over Al-terminated surface, whereas the best packing for the OH-terminated alumina surface is Ag(1 1 1). Both the surface energy and the work function results show that the atomic packing has direct correlation with activity, and hence will certainly influence the reactivity. We therefore need to follow the catalytic reactions over the surface to probe the implications. Silver being a very good oxidation catalyst we are planning to look at some oxidation reactions over the best surfaces identified by this study.

References

[1] D.W.C. Goodman, Model studies in catalysis using surface science probes, Chem. Rev. 95 (1995) 523–536.

[2] B.C. Gates, Supported metal clusters: synthesis, structure, and catalysis, Chem. Rev. 95 (1995) 511–522.

[3] H.J. Freund, Introductory lecture: oxide surfaces, Faraday Discuss. 114 (1999) 1–31.

[4] R.M. Lambert, G. Pacchioni (Eds.), Chemisorptions and Reactivity on Supported Clusters and Thin Films: Towards an Understanding of Microscopic Processes in Catalysis, Kluwer, Dordrecht, The Netherlands, 1997.

[5] M. Gautier, G. Renaud, L.-P. Van, B. Villette, M. Pollak, N. Thormat, F. Jollet, J.P. Duraud, Alpha alumina surfaces—atomic and electronic structure, J. Am. Ceram. Soc. 77 (1994) 323–334.

[6] L. Stara, D. Zeze, V. Matolin, J. Pavluch, B. Gruzza, AES and EELS study of alumina model catalyst supports, Appl. Surf. Sci. 115 (1997) 46–52.

[7] V. Coustet, J. Jupille, High-resolution electron-energy-loss spectroscopy of isolated hydroxyl groups on α-Al_2O_3(0 0 0 1), Surf. Sci. 307–309 (1994) 1161–1165.

[8] H.J. Freund, H. Kuhlenbeck, V. Staemmler, Oxide surfaces, Rep. Prog. Phys. 59 (1996) 283–347.

[9] J.T. Stuckless, D.E. Starr, D.J. Bald, C.T. Cambell, Metal adsorption calorimetry and adhesion energies on clean single-crystal surfaces, J. Chem. Phys. 107 (1997) 5547–5553.

[10] C. Noguera, Physics and Chemistry at Oxide Surfaces, Cambridge University Press, Cambridge, 1996.

[11] G.E. Brown, V.E. Henrich, W.H. Casey, D.L. Clark, C. Eggleston, A. Felmy, D.W. Goodman, M. Grätzel, G. Maciel, M.I. McCarthy, K.H. Nealson, D.A. Sverjensky, M.F. Toney, J.M. Zachara, Metal oxide surfaces and their interactions with aqueous solutions and microbial organisms, Chem. Rev. 99 (1999) 77–174.

[12] M. Causa, R. Dovesi, C. Pisani, C. Roetti, Ab initio Hartree–Fock study of the MgO(0 0 1) surface, Surf. Sci. 175 (1986) 551–560.

[13] C.A. Scamehorn, A.C. Hess, M.I. McCarthy, Correlation corrected periodic Hartree–Fock study of the interactions between water and the (0 0 1) magnesium-oxide surface, J. Chem. Phys. 99 (1993) 2786–2795.

[14] M.I. McCarthy, A.C. Hess, N.M. Harrison, V.R. Saunders, A study of the energetics of the Cl_2/MgO(0 0 1) interface using correlation corrected periodic Hartree–Fock theory, J. Chem. Phys. 98 (1993) 6387–6391.

[15] J.E. Jaffe, N.M. Harrison, A.C. Hess, Ab initio study of ZnO(1 0 1 0) surface relaxation, Phys. Rev. B 49 (1994) 11153–11158.

[16] C. Rehbein, N.M. Harrison, A. Wander, Structure of the alpha-Cr_2O_3(0 0 0 1) surface: an ab initio total-energy study, Phys. Rev. B 54 (1996) 14066–14070.

[17] W.C. Mackrodt, C. Noguera, Bulk and (1 0 0) surface d → d excitation energies in NiO from first-principles Hartree–Fock calculations, Surf. Sci. 457 (2000) L386–L390.

[18] F. Kirchhoff, J.M. Holender, M.J. Gillian, Structure, dynamics, and electronic structure of liquid Ag–Se alloys investigated by ab initio simulation, Phys. Rev. B 54 (1996) 190–202.

[19] W. Langel, M. Parrinello, Ab initio molecular dynamics of H_2O adsorbed on solid MgO, J. Chem. Phys. 103 (1995) 3240–3252.

[20] I. Manassidis, M.J. Gillian, Structure and energetics of alumina surfaces calculated from first principles, J. Am. Ceram. Soc. 77 (1994) 335–338.

[21] J.A. Snyder, J.E. Jaffe, M. Gutowski, Z.J. Lin, A.C. Hess, LDA and GGA calculations of alkali metal adsorption at the (0 0 1) surface of MgO, J. Chem. Phys. 112 (2000) 3014–3022.

[22] P.J.D. Lindan, J. Muscat, S. Bates, N.M. Harrison, M. Gillan, Ab initio simulation of molecular processes on oxide surfaces, Faraday Discuss. 106 (1997) 135–154.

[23] M. Ramamoorthy, D. Vanderbilt, R.D. King-Smith, Defects on TiO_2(1 1 0) surfaces, Phys. Rev. B 49 (1994) 16721–16727.

[24] J. Goniakowski, C. Noguera, Characteristics of Pd deposition on the MgO(1 1 1) surface, Phys. Rev. B 60 (1999) 16120–16128.

[25] M.J. Gillan, P.J.D. Lindan, L.N. Kantorovich, M. Bates, Molecular processes on oxide surfaces studied by first-principles calculations, Miner. Mag. 62 (1998) 669–685.

[26] J.A. Rodriguez, T. Jirsak, S. Sambasivan, D. Fischer, A. Maiti, Chemistry of NO_2 on CeO_2 and MgO: experimental and theoretical studies on the formation of NO_3, J. Chem. Phys. 112 (2000) 9929–9939.

[27] J.A. Rodriguez, S. Azad, L.Q. Wang, J. Garcia, A. Etxeberria, Gonzalez, Electronic and chemical properties of mixed-metal oxides: adsorption and reaction of NO on $SrTiO_3$(1 0 0), J. Chem. Phys. 118 (2003) 6562.

[28] D.C. Sorescu Jr., J.T. Yates, First principles calculations of the adsorption properties of CO and NO on the defective TiO_2(1 1 0) surface, J. Phys. Chem. B 106 (2002) 6184–6199.

[29] D.C. Sorescu, C.N. Rusu Jr., J.T.J. Yates, Adsorption of NO on the TiO_2(1 1 0) surface: an experimental and theoretical study, J. Phys. Chem. B 104 (2000) 4408–4417.
[30] J.A. Snyder, D.R. Alfonso, J.E. Jaffe, Z. Lin, A.C. Hess, M. Gutowski, Periodic density functional LDA and GGA study of CO adsorption at the (0 0 1) surface of MgO, J. Phys. Chem. B 104 (2000) 4717–4722.
[31] J.A. Rodriguez, J.C. Hanson, S. Chaturvedi, A. Maiti, J.L. Brito, Phase transformations and electronic properties in mixed-metal oxides: experimental and theoretical studies on the behavior of $NiMoO_4$ and $MgMoO_4$, J. Chem. Phys. 112 (2000) 935–945.
[32] J.A. Rodriguez, J.C. Hanson, S. Chaturvedi, A. Maiti, J.L. Brito, Studies on the behavior of mixed-metal oxides: structural, electronic, and chemical properties of β-$FeMoO_4$, J. Phys. Chem. B 104 (2000) 8145–8152.
[33] C. Verdozzi, D.R. Jennison, P.A. Schulz, M.P. Sears, Sapphire (0 0 0 1) surface, clean and with d-metal overlayers Phys. Rev. Lett. 82 (1999) 799–1999.
[34] P.J. Eng, T.P. Trainor, G.E. Brown Jr., G.A. Waychunus, M. Newville, S.R. Sutton, M.L. Rivers, Structure of the hydrated α-Al_2O_3(0 0 0 1) surface, Science 288 (2000) 1029–1033.
[35] K.C. Hass, W.F. Schneider, A. Curioni, W. Andreoni, The chemistry of water on alumina surfaces: reaction dynamics from first principles, Science 282 (1998) 265–268.
[36] M. Gazra, N.P. Magtoto, J.A. Kelber, Characterization of oxidized Ni_3Al(110) and interaction of the oxide film with water vapor, Surf. Sci. 519 (2002) 259–268.
[37] P. Liu, T. Kendelewicz, G.F. Brown Jr., E.J. Nelson, S.A. Chambers, Fe_2O_3(0 0 0 1) surfaces: synchrotron X-ray photoemission studies and thermodynamic calculations, Surf. Sci. 417 (1998) 53–65.
[38] S.A. Chambers, T. Droubey, D.R. Jennison, T.R. Matsson, Laminar growth of ultra thin metal films on metal oxides: Co on hydroxylated α-Al_2O_3(0 0 0 1), Science 297 (2002) 827–831.
[39] P. Guenard, G. Renaud, A. Barbier, M. Gautier-Soyer, Determination of the alpha-Al_2O_3(0 0 0 1) surface relaxation and termination by measurements of crystal truncation rods, Surf. Rev. Lett. 5 (1998) 321–324.
[40] D.R. Jennison, T.R. Mattsson, Atomic understanding of strong nanometer-thin metal/alumina interfaces, Surf. Sci. 544 (2003) L689–L696.
[41] J.A. Kelber, C. Niu, K. Shepherd, D.R. Jennison, A. Bogicevic, Copper wetting of α-Al_2O_3(0 0 0 1): theory and experiment, Surf. Sci. 446 (2000) 76–88.
[42] K.C. Hass, W.F. Schneider, A. Curioni, W.J. Andreoni, First-principles molecular dynamics simulations of H_2O on α-Al_2O_3(0 0 0 1), J. Phys. Chem. B 104 (2000) 5527–5540.
[43] A. Bogicevic, D.R. Jennison, Variations in the nature of metal adsorption on ultra thin Al_2O_3 films, Phys. Rev. Lett. 82 (1999) 4050–4053.
[44] A. Chatterjee, T. Iwasaki, T. Ebina, A novel method to correlate layer charge and the catalytic activity of 2:1 dioctahedral smectite clays in terms of binding the interlayer cation surrounded by monohydrate, J. Phys. Chem. A 104 (2000) 8216–8223.
[45] A. Chatterjee, H. Hayashi, T. Iwasaki, First principle study to correlate location and activity of ruthenium oxide incorporated in alkali-metal hexatitanates, J. Phys. Chem. B 105 (2001) 3463–3469.
[46] M.P. Teter, M.C. Payne, D.C. Allen, Solution of Schrödinger's equation for large systems, Phys. Rev. B 40 (1989) 12255–12263.
[47] M.C. Payne, M.P. Teter, D.C. Allen, T.A. Arias, J.D. Johannopoulos, Iterative minimization techniques for ab initio total-energy calculations—molecular dynamics and conjugate gradients, Rev. Mod. Phys. 64 (1992) 1045–1097.
[48] D. Vanderbilt, Soft self-consistent pseudopotentials in a generalized eigenvalue formalism, Phys. Rev. B 41 (1990) 7892–7895.
[49] J. Perdew, A. Zunger, Self-interaction correction to density-functional approximations for many-electron systems, Phys. Rev. B 23 (1981) 5048–5079.
[50] B. Winkler, V. Milman, M.C. Payne, Orientation, location, and total energy of hydration of channel H_2O in corderite investigated by ab initio total-energy calculation, Am. Mineral. 79 (1994) 200–204.
[51] J.P. Perdew, Density-functional approximation for the correlation energy of the inhomogeneous electron gas, Phys. Rev. B 33 (1986) 8822–8824.
[52] A.D. Becke, Density functional exchange energy approximation with correct asymptotic behavior, Phys. Rev. A 38 (1988) 3098–3100.
[53] H.J. Monkhorst, J.D. Pack, Special points for Brillouin-zone integrations, Phys. Rev. B 13 (1976) 5188–5192.
[54] W. Wang, K. Fan, J. Deng, Structural and electronic properties of silver surfaces: ab initio pseudopotential density functional study, Surf. Sci. 490 (2001) 125–132.
[55] J.M. Wittbrodt, W.L. Hase, H.B. Schelgel, Ab initio study of the interaction of water with cluster models of the aluminum terminated (0 0 0 1) α-aluminum oxide surface, J. Phys. Chem. B 102 (1998) 6539–6548.
[56] Y. Wang, X.-G. Wang, A. Chaka, M. Scheffer, The hematite (alpha-Fe_2O_3) (0 0 0 1) surface: evidence for domains of distinct chemistry, Phys. Rev. Lett. 81 (2000) 1038–1041.
[57] I.G. Batirev, A. Alavi, M.W. Finnis, T. Deutsch, First-principles calculations of the ideal cleavage energy of bulk niobium(1 1 1)/alpha-alumina(0 0 0 1) interfaces, Phys. Rev. Lett. 82 (1999) 1510–1513.
[58] P. Guenard, G. Renaud, A. Barbier, M. Gautier-Soyer, Mater. Res. Soc. Symp. Proc. 437 (1996) 15.
[59] P.H.T. Philipsen, E. Baerends, Relativistic calculations to assess the ability of the generalized gradient approximation to reproduce trends in cohesive properties of solids, Phys. Rev. B 61 (2000) 1773–1778.
[60] E. Krotscheck, W. Kohn, Nonlocal screening in metal surfaces, Phys. Rev. Lett. 57 (1986) 862–865.
[61] M. Chelvayohan, C.H.B. Mee, Work function measurements on (1 1 0), (1 0 0) and (1 1 1) surfaces of silver, J. Phys. C: Solid State Phys. 15 (1982) 2305–2312.
[62] L. Vattuone, M. Rocca, C. Boragno, U. Valbusa, Initial sticking coefficient of O_2 on Ag(1 1 0), J. Chem. Phys. 101 (1994) 713–725.